Capacity of Sun-driven Lunar Swingby Sequences and Their Application in Asteroid Retrieval

Chen, Hongru
Department of Aeronautics and Astronautics, Kyushu University : Assistant Professor

出版情報：Astrodynamics, 2023-04-11. Tsinghua University Press
バージョン：
権利関係：

Capacity of Sun-driven Lunar Swingby Sequences and Their Application in Asteroid Retrieval

Hongru Chen[1](✉)

1. Department of Aeronautics and Astronautics, Kyushu University, Fukuoka, 8190395, Japan

✉ hongru.chen@hotmail.com

Received: 15 December 2022 / Accepted: 21 Feburary 2023

Abstract

For deep-space mission design, the gravity of the Sun and the Moon can be first considered and utilized. Their gravity can provide the energy change for launching spacecraft and retrieving spacecraft as well as asteroids. Regarding an asteroid retrieval mission, it can lead to the mitigation of asteroid hazards and an easy exploration and exploitation of the asteroid. This paper discusses the application of the Sun-driven lunar swingby sequence for asteroid missions. Characterizing the capacity of this technique is not only interesting in terms of the dynamic insights but also non-trivial for trajectory design. The capacity of a Sun-driven lunar swingby sequence is elucidated in this paper with the help of the "Swingby-Jacobi" graph. The capacity can be represented by a range of the Jacobi integral that encloses around 660 asteroids currently cataloged. To facilitate trajectory design, a database of Sun-perturbed Moon-to-Moon transfers, including multi-revolution cases is generated and employed. Massive trajectory options for spacecraft launch and asteroid capture can then be explored and optimized. Finally, a number of asteroid flyby, rendezvous, sample-return, and retrieval mission options enabled by the proposed technique are obtained.

Keywords

Asteroid mining · Planetary defense · Gravity assists · Moon-to-Moon transfers · Reachable sets · Graphical methods

Nomenclature

NRHO	near-rectilinear halo orbit
SPMT	Sun-perturbed Moon-to-Moon transfer
GTO	geostationary transfer orbit
SE	Sun-Earth
CR3BP	circular-restricted three-body problem
GNC	guidance, navigation, and control operations
Δv	impulsive velocity increment
$\mathbf{v}_\infty$, v_∞	vector and magnitude of the hyperbolic excess velocity with respect to a celestial body
M, E	subscripts indicating references to the Moon and the Earth, respectively
φ	swingby pump angle
δ	declination of the escape or incident trajectory
C_3	characteristic energy (also v_∞^2) with respect to Earth
J	Jacobi integral in the SE-CR3BP
ToF	time of flight
$\mathcal{A}$	reachable set with a Sun-driven lunar swingby sequence
$\mathcal{A}_\mathrm{p}$	reachable set with a planar swingby sequence
$\mathcal{B}$	reachable domain of $v_{\infty\mathrm{E}}$ and δ

1 Introduction

In space mission and trajectory design, gravity assists and low-energy transfers that take advantage of the gravity of celestial bodies are often employed to reduce fuel consumption as well as increase the mass of payloads. For all missions that depart from Earth, the Moon is the closest celestial body that can provide a gravity assist. In fact, in the Sun-Earth-Moon system a spacecraft is influenced by the joint gravitational effect from the Sun, the Earth, and the Moon. Trajectory design for missions such as the HITEN, ARTEMIS-THEMIS, NOZOMI, DESTINY, EQUULEUS, and Lunar Flashlight have employed lunar swingbys driven by solar tides [1–7]. The joint gravitational effect can assist the launch of a spacecraft and the capture of the returning spacecraft as well as samples from the visited body. However, the joint gravitational effect has not yet been well characterized for mission analysis and trajectory design.

In this paper, the capacity of a Sun-driven lunar swingby sequence and its application for asteroid retrieval will be clarified.

Asteroids are considered to be promising bonanza that may contain water and rare metals. These resources can be used to sustain astronauts' lives, fuel spacecraft as well as power space bases. Developments on Earth can also benefit from asteroid mining. Furthermore, asteroids are of great scientific interest as they preserve pristine relics of the early solar system. Missions such as DAWN, NEAR, Hayabusa-1 and -2, and Osiris-REx have returned significant information and even samples that led to a better understanding of asteroids and the early solar system. An increasing number of missions, such as LUCY, PSYCHE, and MMX, will be visiting asteroids and asteroid-like small bodies. However, near-Earth asteroids (NEA) can be threats to Earth due to the constant possibility of Earth impacts. The Chelyabinsk meteor should be considered a warning. It is time to "look up" and tackle potential asteroid attacks. NASA and ESA are working on the DART and HERA missions to demonstrate asteroid deflection technologies [8, 9]. In this context, the concept of asteroid retrieval has also been proposed. Asteroid retrieval has the goal of bringing an asteroid or a part of it into the vicinity of the Earth. That will not only mitigate the threat but also allows for easy and constant visits to the asteroid. Moreover, the technology necessary for retrieving asteroids becomes more realistic. For instance, retrieving an entire small NEA – with a diameter of approximately 7 m and a mass on the order of 500,000 kg is believed to be possible by 2025 [10].

Asteroid retrieval was investigated from the perspectives of propulsion technologies and trajectory design in several studies. In this paper, the problem is discussed from the perspective of trajectory design. In this frame, the Sun-Earth libration-point orbits have been proposed for capturing asteroids [11–14]. As this method mostly relies on natural capture by the gravity of the Sun and the Earth, it takes considerable time or Δv to retrieve a target. In addition, libration-point orbits are not stable. Constant station-keeping maneuvers are needed, which is not feasible in the long run. Without stationkeeping, the captured asteroid could become a serious hazard to Earth. A lunar swingby can change the orbital energy more effectively. Landau et al. (2013) [15] and Gong and Li (2015) [16] proposed using lunar swingbys. Using this method, the v_∞ with respect to the Moon is considered invariable, and resulting orbits with their apogees beyond the Moon's orbit will be constantly influenced by lunisolar perturbations, which are unstable and threatening to Earth. For stable capture, not only does the characteristic energy with respect to Earth have to be minimized, but also the v_∞ with respect to the Moon. Urrutxua et al. (2015) [17] included the gravity of the Moon in the Sun-Earth Hill's problem, and ran extensive simulations to reveal temporary capture trajectories prolonged by tens to hundreds of meters per second of Δv. Nevertheless, a concrete

characterization of easily capturable orbit types (or objects) under the gravity of the Sun, the Earth, and the Moon, is still lacking.

The Sun-driven lunar swingby sequence investigated in this paper can change the v_∞ with respect to both the Earth and the Moon, and thus can be used for launching spacecraft and capturing asteroids into a high lunar orbit or the Earth-Moon near-rectilinear halo orbit (NRHO), which is stable to the Earth. In this paper, the retrieval mission is considered in three phases. In the vicinity of the Earth, for the escape phase, a Sun-driven lunar swingby sequence is utilized to increase the v_∞ of the spacecraft with respect to Earth, as well as target a certain direction for the asteroid. For the capture phase, a Sun-driven lunar swingby sequence is used to reduce the v_∞ of the asteroid with respect to the Moon to an acceptably low level, which allows for an inexpensive insertion into orbits stably confined to the Moon. In the heliocentric transfer phase, the spacecraft rendezvous with the targeted asteroid, and the asteroid is sent back to Earth with permissible Δv. There are around 15000 NEA currently cataloged. Searching and optimizing possible heliocentric transfer and swingby sequences each time the asteroid database is updated is computationally expensive and time-consuming. It is often desired to characterize the capacity (i.e., referred to as the reachable set, attainable set, or attractive set in the literature) of certain trajectory design methods for the purposes of obtaining initial guesses, pruning the search space, etc. (e.g., Ref. [18–22]). Regarding the problem of interest in this paper, characterizing the capacity of Sun-driven lunar swingby sequences for reaching and capturing heliocentric objects is not only interesting in terms of dynamic insights but also non-trivial for mission planning.

Graphical methods are sometimes helpful for trajectory design and analysis. Strange and Longuski (2002) [23] proposed the Tisserand graph with v_∞ contours for analyzing and planning gravity-assist sequences. It is based on the patched two-body approximation. The Poincaré map is useful in analyzing the three-body problem. Campagnola and Russell (2010) [24] further developed the Tisserand-Poincaré graph with the Tisserand (or Jacobi) contours that consider the third-body perturbation during a swingby. Ross and Scheeres (2007) [25] proposed the periapsis-Poincaré map for analyzing low-energy capture and escape. Those graphs are applicable for star-planets and planet-moons systems. For the star-planet-moon system concerned in this work, the Swingby-Jacobi graph developed by Chen et al. (2016) [5] and Chen (2017) [26] is applicable. In addition to the Jacobi integral in the Sun-Earth system, the effect of lunar swingbys can also be portrayed. The double Tisserand graph recently developed by Martens and Bucci (2022) [27] is notable and also applicable for the star-planet-moon system. The double Tisserand graph is suitable for analyzing transfers to the moon, while the Swingby-Jacobi graph is suitable for analyzing

transfers to the heliocentric region. The Swingby-Jacobi graph is adopted in this paper for elucidating the accessibility of a Sun-driven lunar swingby sequence to the heliocentric region.

This paper is organized as follows. In Sec. 2, the dynamic model used for trajectory design and the mechanism of the sequence of Sun-perturbed Moon-to-Moon transfers (SPMT) and lunar swingbys for enhancing mission design are presented. The Swingby-Jacobi graph is also introduced to visualize the effects of Sun-perturbed transfers and lunar swingbys. Sec. 3 elucidates the capacity of a Sun-driven lunar swingby sequence with the help of the Swingby-Jacobi graph. It is characterized by an accessible range of the Jacobi integral and an accessible domain of the magnitude and declination of the $\mathbf{v}_\infty$ with respect to Earth. These ranges effectively exclude the definitely inaccessible asteroids and inaccessible heliocentric transfer options from among the optimized. The computation routine for optimal heliocentric transfers is presented in Sec. 4.1. To facilitate patching SPMT segments and lunar swingbys for meeting the escape or capture conditions, a database of SPMT solutions is established. The effort of computing the database is described in Sec. 4.2.1. With the characterized capacity of this technique and the trajectory design tools, lists of possible asteroid flyby, rendezvous, sample-return, and retrieval missions for the next 20 years are obtained, which are presented in Sec. 5. Disadvantages and advantages of different Moon-to-Moon transfer types, namely the short transfer, Sun-perturbed transfer, and three-dimensional transfer, are discussed in Sec. 6. Conclusions are given in the last section.

2 Dynamic Model and Swingby-Jacobi Graph

2.1 Dynamic Model

The motions of spacecraft and asteroid samples in the vicinity of the Earth are influenced by the gravity of the Sun, the Earth, and the Moon. To facilitate analysis and orbit design, the patched Sun-Earth circular restricted three-body problem (SE-CR3PB) and lunar swingby model is adopted. The synodic coordinate system, in which the Sun-Earth barycenter is put at the origin and the Sun and Earth are fixed on the x-axis, and the rotation direction is aligned with the z-axis, as shown in Fig. 1, is used. Let μ denote the ratio of the mass of the Earth to the total mass of the two bodies, the distance between the Sun and the Earth, AU, be the length unit, and the time unit is set in the way that the period of the Earth's becomes

2π. Then, the equations of motion in the SE-CR3BP are expressed as:

$$\ddot{x} - 2\dot{y} = \partial U/\partial x \tag{1}$$

$$\ddot{y} + 2\dot{x} = \partial U/\partial y \tag{2}$$

$$\ddot{z} = \partial U/\partial z \tag{3}$$

where U denotes the pseudo-gravitational potential expressed as:

$$U = (x^2 + y^2)/2 + (1-\mu)/r_1 + \mu/r_2 \tag{4}$$

where $\mu = 3.003\,5 \times 10^{-6}$ for the Sun-Earth system, and the distances are:

$$r_1 = \sqrt{(x+\mu)^2 + y^2 + z^2}, \quad r_2 = \sqrt{(x-1+\mu)^2 + y^2 + z^2} \tag{5}$$

An energy quantity, known as the Jacobi integral, holds in the CR3BP system. The Jacobi integral J is expressed as:

$$J = (\dot{x}^2 + \dot{y}^2 + \dot{z}^2) - 2U \tag{6}$$

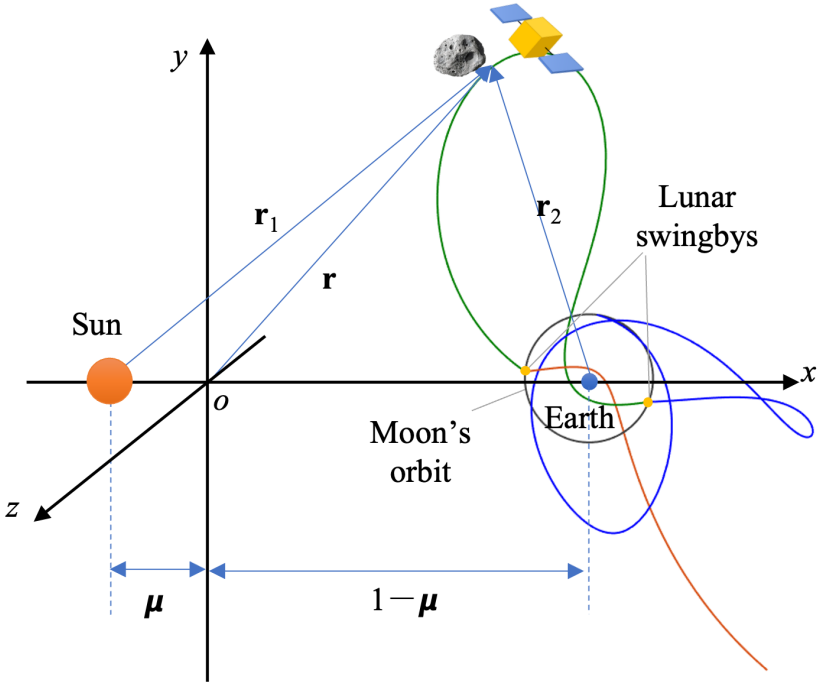

Fig. 1 Schematic of the patched Sun-Earth CR3BP and lunar swingby model.

Trajectories are considered in the SE-CR3BP most of the time. The lunar gravity is approximated by the lunar swingby, which is only effective at a lunar encounter. In other words, the object receives

an instantaneous velocity change (i.e., $\mathbf{v}_\infty$ with respect to the Moon gets an instantaneous bend) at a lunar encounter. The inclination and eccentricity of the Moon's orbit are small and are set to zero in this simplified model. Such a SE-CR3BP plus lunar swingby model is schematically depicted in Fig. 1.

2.2 Sun-perturbed Moon-to-Moon transfers

For a trajectory to be seen as an Earth orbit, the v_∞ with respect to the Moon, $v_{\infty\mathbf{M}}$, remains constant, if solar gravity is not taken into account. In the presence of solar perturbations, $v_{\infty\mathbf{M}}$ will be changed as the "Earth" orbit reaches a far region where solar perturbations are significant. To illustrate, Fig. 2 schematically depicts the solar tidal force in the Earth-centered inertial frame and its effect on orbits around the Earth. As shown, after the first lunar swingby (S1), or an outward crossing of the Moon's orbit, the resulting orbit with its apogee far away in the 1st or 3rd quadrants will experience posigrade deceleration near the apogee, and come back to a second lunar swingby (S2) with a larger encounter angle α with respect to the Moon's orbit, and can even be in the retrograde direction. Even though the velocity is decreased (considering the posigrade situation), $v_{\infty\mathbf{M}}$ is still increased because of the increased α. This mechanism is further clarified via the Swingby-Jacobi graph introduced in the next section. In contrast, an orbit with its apogee in the 2nd or 4th quadrants will experience acceleration, resulting in a decreased $v_{\infty\mathbf{M}}$ at S2 or missing the Moon's orbit. Such Sun-perturbed Moon-to-Moon transfers (hereafter referred to as SPMT or Sun-perturbed M-M transfers) can be employed to improve the lunar encounter condition for a gravity-assisted escape, as planned for the NOZOMI and DESTINY missions [3–5]. Furthermore, they can be used for an inexpensive insertion into a lunar orbit, as applied in the HITEN, ARTEMIS-THEMIS, EQUULEUS, and Lunar Flashlight missions [1, 2, 6, 7].

2.3 Swingby-Jacobi graph

Given $v_{\infty\mathrm{M}}$ and the pump angle φ (i.e., angle between the $\mathbf{v}_{\infty\mathrm{M}}$ and the Moon's velocity $\mathbf{v}_\mathrm{M}$ vectors) one can compute the Jacobi integral J in the SE-CR3BP. Although J can vary with the position of the lunar encounter and the out-of-plane degree of $\mathbf{v}_{\infty\mathrm{M}}$, these factors only change the Jacobi integral within an insignificant range. Figure 3 shows contours of J on the $v_{\infty\mathrm{M}}$-φ plane. In this graph, a lunar swingby can be portrayed by the vertical motion of a state (blue dot), which changes J in the Sun-Earth system. The following M-M transfer can be perturbed by the Sun, while J is maintained. Solar perturbations can be portrayed by motions along the Jacobi contours. The Jacobi contours and the $v_{\infty\mathrm{M}}$-φ plane constitute the basis of the "Swingby-Jacobi" graph. Orbital information can be added to this graph, which enables

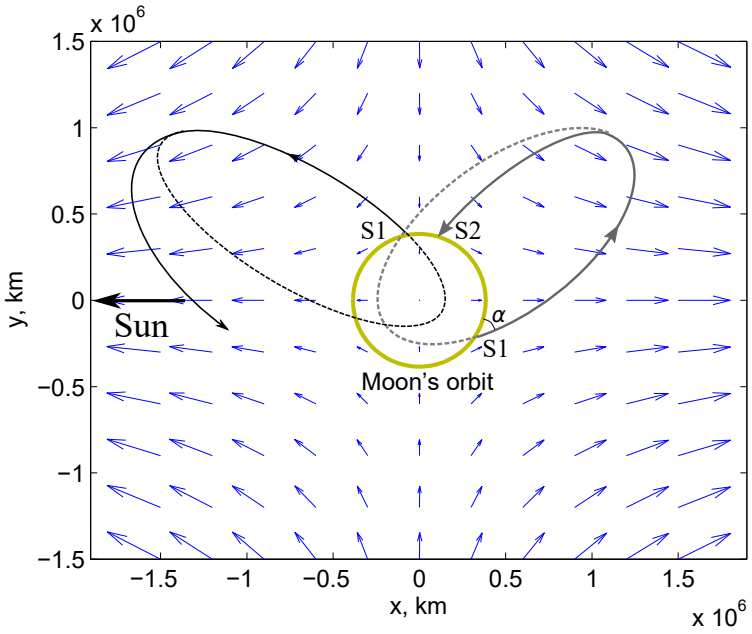

Fig. 2 The solar gravitational influence on orbit states with respect to the Earth and the Moon (figure reused from Ref. [5, 26]).

insights into the orbit dynamics and effects on the mission. Figure 3 includes contours of the encounter angle α and osculating (i.e., at the lunar encounter) characteristic energy C_3 (i.e., v_∞^2) with respect to Earth. It can be seen that in the direction that C_3 is slightly decreased and α is increased, which corresponds to the situation of posigrade deceleration in the 1st and 3rd quadrants, $v_{\infty\mathrm{M}}$ is increased. This visualizes and explains the mechanism by which $v_{\infty\mathrm{M}}$ increases while C_3 decreases during a Sun-perturbed transfer. To conclude, the following situations are visualized in the graph.

- The orbital energy with respect to Earth, represented by C_3, is influenced by lunisolar perturbations;
- The Jacobi integral in the Sun-Earth three-body problem, represented by J, is influenced by lunar gravity;
- The orbital energy with respect to the Moon, represented by $v_{\infty\mathrm{M}}$, is influenced by solar gravity;
- $v_{\infty\mathrm{M}}$ is increased after a Sun-perturbed transfer mainly in the 1st and 3rd quadrants, and decreased after a Sun-perturbed transfer in the 2nd and 4th quadrants.

Therefore, a sequence of Sun-perturbed M-M transfers and lunar swingbys can be utilized 1) to assist escape and asteroid encounter, namely, to achieve certain C_3, J, and escape directions, and 2) for asteroid capture, namely, to reduce $v_{\infty\mathrm{M}}$ for inexpensive lunar orbit insertion. Other information can also be added to this graph. For instance, the maximum post-swingby C_3 is also a function of the pre-swingby φ and $v_{\infty\mathrm{M}}$, and thus can be plotted in the Swingby-Jacobi graph. Given an initial state, the achievable C_3 after

two swingbys can be revealed, which is presented in Ref. [5]. The characterization of the capacity of a Sun-driven lunar swingby sequence in Sec. 3.1 is aided by this graph.

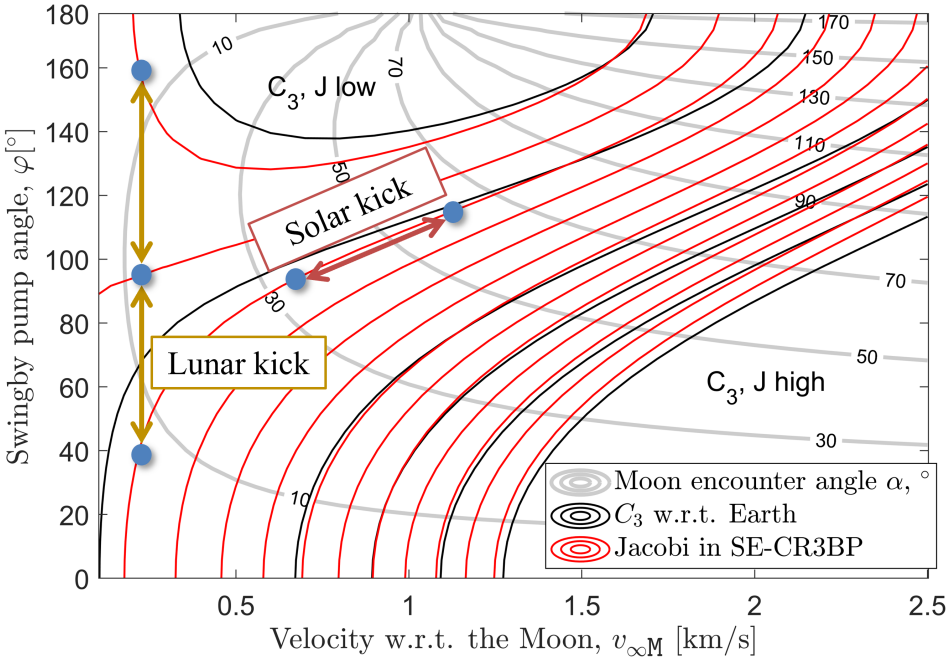

Fig. 3 Swingby-Jacobi graph

2.4 Trajectory design objectives

It is therefore feasible to launch a spacecraft with a low initial $v_{\infty M}$ into deep space, and to reduce the $v_{\infty M}$ of a returned spacecraft and asteroid samples for an inexpensive insertion into a stable lunar orbit, using the Sun-driven lunar swingby sequence. A low-cost initial $v_{\infty M}$ (i.e., before acceleration via a Sun-driven lunar swingby sequence) is commonly between 200 m/s (i.e., via a low-thrust spiral orbit raising) and 800 m/s (i.e., via a direct transfer from a GTO). Therefore, for an Earth escape that targets an asteroid, the objective of trajectory design is to minimize the initial $v_{\infty M}$ to below 800 m/s. For spacecraft and asteroid capture, the objective is to achieve a final $v_{\infty M}$ smaller than 450 m/s, enabling insertion into a mid- to high-lunar orbit at a Δv of around 350 m/s or a stable NRHO at 20 m/s [7, 28, 29]. Another propulsion system launched to the Earth-Moon regime years later can possibly provide this insertion Δv while waiting to dock with the returned spacecraft and asteroid.

3 Capacity of Sun-driven lunar swingby sequences

There are around 15,000 cataloged near-Earth asteroids. Each one has hundreds of locally optimal heliocentric transfer trajectories from and to the Earth's vicinity in any given interval of 20 years. Each Earth escape or Earth encounter condition leads to hundreds to thousands of possible lunar swingby sequences given the computed database of SPMT (introduced in Sec. 4.2.1) and a limit of two SPMT segments. Computing all possible trajectories each time the asteroid database is updated can be very time-consuming. Therefore, it is desired to reduce the search space based on the capacity of a Sun-driven lunar swingby sequence.

3.1 Accessible energy range

Looking at the Swingby-Jacobi graph, it may seem that an orbit state can be freely moved between the left side (i.e., small $v_{\infty \mathrm{M}}$) and the right side (i.e., large $v_{\infty \mathrm{M}}$). However, as $v_{\infty \mathrm{M}}$ increases, the bending angle of $\mathbf{v}_{\infty \mathrm{M}}$ becomes more restricted, and so does the Jacobi jump. When $v_{\infty \mathrm{M}}$ is large (i.e., $>$ 2.5 km/s), it can take many segments of SPMTs and lunar swingbys to substantially reduce or increase $v_{\infty \mathrm{M}}$. Additionally, when $v_{\infty \mathrm{M}}$ is large, C_3 with respect to Earth is inevitably large, and the SPMT is in a hyperbolic arc whose ToF is generally longer than 200 days. Therefore, using the Sun-driven lunar swingby sequence is not efficient when C_3 and $v_{\infty \mathrm{M}}$ are large.

Time is a critical factor for space missions. In this work, the ToF of an M-M transfer is limited to 200 days, and the number of patched SPMTs is limited to 2. The ToF constraint essentially restricts the maximum accessible C_3. For all SPMTs limited by 200 days that have been solved for the database, C_3 is generally below 0 (although a few solutions reach 0.7 km^2/s^2). Therefore, a constraint is applied that limits C_3 to 0 before the last (or after the first) lunar swingby for escape (or capture) purposes. Additionally, the limit of the bending angle γ of $\mathbf{v}_{\infty \mathrm{M}}$ at a lunar swingby constrains the maximum pre-swingby or post-swingby C_3, $C_{3\,\max}$. γ is limited by [30],

$$\gamma_{\max} = \pi - 2 \times \arccos\left[G_{\mathrm{M}}/(G_{\mathrm{M}} + r_{\min} \cdot v_{\infty \mathrm{M}}^2)\right] \tag{7}$$

where G_{M} is the gravitational parameter of the Moon and $r_{\min}$ is the minimum flyby radius, which is set to 1838 km (i.e., 100 km above the surface of the Moon). This constraint also restricts the capacity of a Sun-driven lunar swingby sequence.

To express the effects of those constraints, the $C_3 = 0$ contour is highlighted on the Swingby-Jacobi graph, as shown in Fig. 4. For $C_3 = 0$, the corresponding φ which leads to the maximum pre-swingby or

post-swingby C_3 while being constrained by $\gamma_{\max}$ is plotted as a blue line on the graph. The area bounded by these two lines indicates the accessible heliocentric orbit states after or before a Sun-driven lunar swingby sequence. The maximum accessible J is obtained at the tangent point (annotated by a circle in Fig. 4) of the $C_{3\,\max}$ boundary (blue) and the Jacobi contours, which is -2.9965. The loosely equivalent C_3 is 3.3 km^2/s^2, and the v_∞ with respect to Earth, $v_{\infty\mathrm{E}}$, is 1.8 km/s. In addition, orbits of low J may pass by the Earth through the Sun-Earth Lagrangian L_1 point, where $J = -3.0009$. The accessible J indicates the accessible heliocentric orbits, as the Jacobi integral can be expressed in the Tisserand form as a function of the orbital elements (for more detail, see Ref. [31]), which is,

$$J = -(1-\mu)/a - 2\sqrt{a(1-\mu)(1-e^2)} \times \cos i \tag{8}$$

where a, i, and e are the semi-major axis, inclination, and eccentricity of a heliocentric orbit, respectively. The reachable set $\mathcal{A}$ with a Sun-driven lunar swingby sequence can be expressed as:

$$\mathcal{A} \supset \{(a,e,i) | -3.0009 < J < -2.9965\} \tag{9}$$

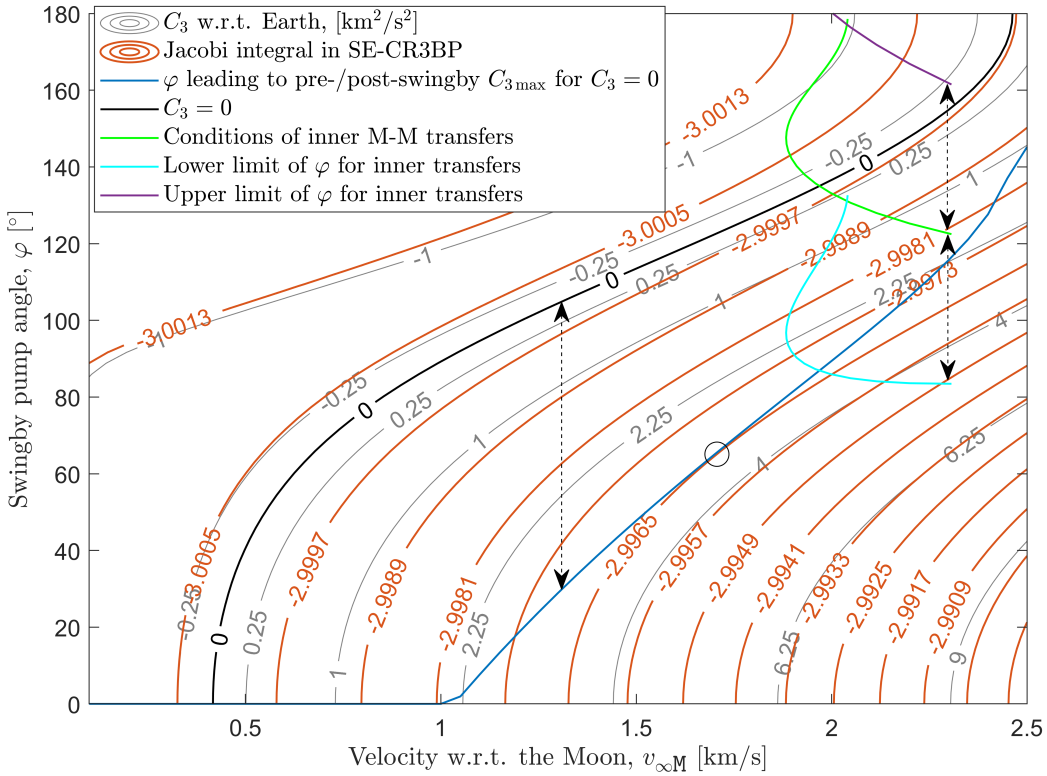

Fig. 4 To reveal the capacity of a Sun-driven lunar swingby sequence in terms of the accessible Jacobi range.

The superset above means that there is another possibility to further expand the accessible heliocentric region. McElrath et al. (2012) [32] discussed the application of the retrograde inner M-M transfer. This kind of transfer is short (i.e., 4 to 15 days) and inside the Moon's orbit, and thus is not considered as a Sun-perturbed transfer. The $v_{\infty \mathrm{M}}$ is thus the same at the two consecutive lunar encounters. Some of these transfers are hyperbolic arcs. To illustrate its useful features for the problem of interest, the solutions of inner transfers are manifested as a green curve in Fig. 4. The lower end is associated with the minimum Earth flyby altitude, which is 220 km in this work. The orbit state can be considered to jump twice vertically as a result of the two consecutive lunar swingbys of this transfer. Therefore, boundaries of the φ leading to and resulting from the swingbys of the inner M-M transfers are also plotted in Fig. 4. The orbit state above the lower φ boundary (cyan) can be transferred from or to a state with $C_3 < 0$ with the two lunar swingbys at the ends of a short inner transfer. Therefore, this kind of transfer provides another accessible area in the heliocentric region, which is a triangle-like area outside the aforementioned blue boundary. It can be read out that the accessible J is up to -2.9946, which is loosely equivalent to a C_3 of 4.83 km^2/s^2 and a $v_{\infty \mathrm{E}}$ of 2.2 km/s. However, the distribution of this level of J is not isotropic in space. The reason is that the inner M-M transfer requires bending the escape (or incident) trajectory from (or onto) the ecliptic plane, and the constraint on the bending angle increases with velocity. This will be further analyzed in the next subsection. Then, the reachable set is a subset expressed as:

$$\mathcal{A} \subset \{(a, e, i) | -3.0009 < J < -2.9946\} \tag{10}$$

3.2 Accessible direction range

To use the inner M-M transfer, it should be connecting the lunar swingby sequence and the heliocentric trajectory, namely, as the last segment of the escape phase, or the first segment of the capture phase. This requires the last (or the first) swingby to bend the $\mathbf{v}_{\infty \mathrm{M}}$ from (or onto) the ecliptic plane given a targeted escape (or incident) $\mathbf{v}_{\infty}$ with respect to Earth, $\mathbf{v}_{\infty \mathrm{E}}$, which may not be in the plane.

If only SPMTs are employed, it is also preferred to bend the last (or first) $\mathbf{v}_{\infty \mathrm{M}}$ from (or onto) the plane. As reasoned in Sec. 6.2, three-dimensional SPMTs do not result in significant changes in $v_{\infty \mathrm{M}}$ and thus are not efficient given the constraint on ToF and the number of SPMTs. Because of the bending angle constraint, the escape (or capture) condition becomes more difficult to achieve as the targeted declination of $\mathbf{v}_{\infty \mathrm{E}}$ increases. It is thus necessary to derive the relationship between the accessible ranges of the magnitude $v_{\infty \mathrm{E}}$ and the declination δ of $\mathbf{v}_{\infty \mathrm{E}}$.

The escape and incident $\mathbf{v}_{\infty \mathrm{E}}$ can be related to an Earth orbit. Note that the solar perturbation is

not considered in the escape and incident arc (i.e., connecting the heliocentric phase and the swingby sequence), because of its short effect and for the sake of simplicity. The corresponding Earth orbit has an inclination ranging from δ to 90°. The inclination is determined by the difference between the ascension of $\mathbf{v}_{\infty \mathrm{E}}$ and the lunar phase at the lunar encounter. For the same $v_{\infty \mathrm{E}}$ and thus the same velocity at the lunar encounter, and the same $v_{\infty \mathrm{M}}$, a low-inclination orbit results in a lower declination of $\mathbf{v}_{\infty \mathrm{M}}$ than a high-inclination orbit (see illustration in Fig. 5). It is more difficult to bend the $\mathbf{v}_{\infty \mathrm{M}}$ of a higher declination from (or onto) the plane.

To examine the accessible situation for an escape (incident) vector of certain $v_{\infty \mathrm{E}}$ and δ, one can vary the lunar encounter position, compute the orbit state at the encounter (i.e., see Appendix) and the bending angle limit (Eq. 7), and examine whether the orbit state at the encounter can be bent from (or to) the ecliptic plane with $C_3 < 0$. By examining various lunar encounter phases, $v_{\infty \mathrm{E}}$, and δ, a two-dimensional accessible area is revealed, as shown in Fig. 6. In addition, the situation with one inner M-M transfer in the sequence is considered. The possibility of this situation is dependent on whether the state can be bent from (or onto) the solution of the inner transfer (i.e., depicted by the green line in Fig. 4). The corresponding boundary is also shown in Fig. 6. Let the combined accessible domain in Fig. 6 be denoted by a set $\mathcal{B}$. The reachable set with a planar Sun-driven lunar swingby sequence, $\mathcal{A}_{\mathrm{p}}$, can be expressed as,

$$\mathcal{A}_{\mathrm{p}} = \{(a, e, i) | (v_{\infty \mathrm{E}}, \delta) \in \mathcal{B}\} \tag{11}$$

While the orbital elements can be loosely mapped from $v_{\infty \mathrm{E}}$ and δ, because $\mathcal{B}$ cannot be expressed as a single function, characterizing Eq. 11 into explicit functions is not specifically performed in this work. Instead, Eq. 10 is used to pre-select potential candidates, and Eq. 11 is used in a later step to verify the true accessibility, as is demonstrated in Sec. 5.

Figure 6 also shows that a Sun-driven lunar swingby sequence (constrained by ToF and the number of SPMTs) can at least achieve or absorb a $v_{\infty \mathrm{E}}$ of up to 1.46 km/s in all directions. The corresponding C_3 is 2.13 $\mathrm{km}^2/\mathrm{s}^2$, and the loosely equivalent J is -2.9980. Thus, $\mathcal{A}_{\mathrm{p}}$ contains the subset associated with this Jacobi range, which is expressed as,

$$\mathcal{A}_{\mathrm{p}} \supset \{(a, e, i) | -3.0009 < J < -2.9980\} \tag{12}$$

3.3 Potentially accessible asteroids

Because a spacecraft does not generally rendezvous with an asteroid, a Δv to stop it at the asteroid, denoted by Δv_{stop}, is required. Similarly, an asteroid does not commonly reach the Earth's vicinity without a Δv to

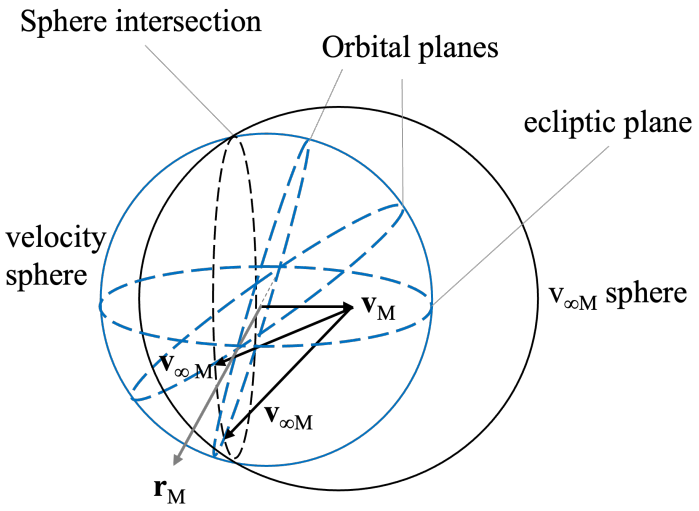

Fig. 5 Lunar encounter situations for specified velocity and $v_{\infty \mathrm{M}}$.

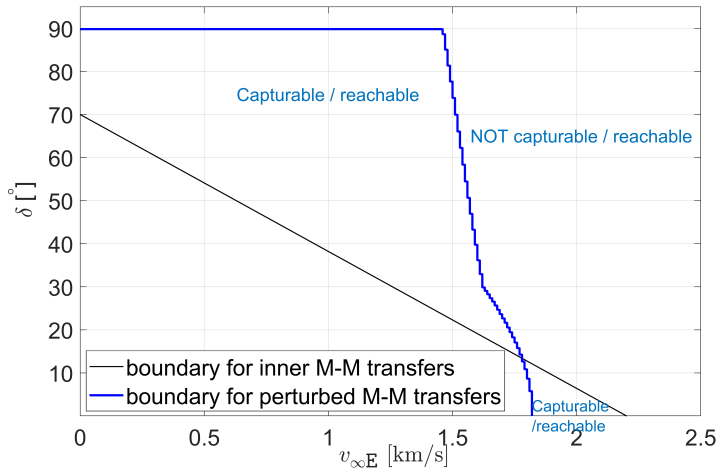

Fig. 6 Accessible domain of the $\mathbf{v}_{\infty \mathrm{E}}$ magnitude and its declination.

return it, denoted by Δv_{retn}. Nevertheless, asteroids whose orbits are outside the reachable set cannot be reached or returned with a small Δv as the expected large velocity difference at the intersection needs to be canceled. Therefore, the characterized capacity of a Sun-driven lunar swingby sequence also indicates the easily accessible targets. To show the increased capacity with the proposed method, a comparison with the methods using lunar swingbys and the Sun-Earth libration dynamics on the accessible Jacobi and the corresponding number of potential targets in the current asteroid database is presented in Table 1.

Δv_{stop} and Δv_{retn} are limited to a small amount, such that the effect of the gravity assists is still dominant and we do not depart from the idea of easily reachable and retrievable asteroids. For reaching the target, a Δv_{stop} budget of 1 km/s is assumed to be available. For retrieving the spacecraft and samples

Table 1 Comparison of different gravity-assist methods

Method		Accessible Jacobi	Number of candidates [d]
Lunar swingbys		[-3.0009, -2.9962] [a]	491
S-E libration-point dynamics		[-3.0009, -2.9992] [b]	168
Sun-driven lunar swingby sequence	only SPMTs	[-3.0009, -2.9965] [c]	456
	with an inner transfer	[-3.0009, -2.9946] [c]	657

[a] Gong and Li (2015) [16]

[b] Sanchez and Garcia Yarnoz (2016) [14]

[c] The present work and Chen (2017) [26]

[d] Based on the database of the Minor Planet Center: https://minorplanetcenter.net/iau/MPCORB/MPCORB.DAT, accessed on 2022 Aug. 15.

from the target, a Δv_{retn} budget of 500 m/s is assumed to be available. These Δv budgets can also enable low energy asteroids to reach Sun-Earth L_1 and pass by the Earth, and thus alter the lower bound of the accessible Jacobi range. After subtracting the kinetic energy attributed to the Δv budget from the J at L_1, the lower bound of the J of a reachable asteroid becomes -3.0020, and that of a retrievable one becomes -3.0012. These Jacobi ranges are applied in the first place to exclude the definitely inaccessible asteroids.

4 Trajectory design

4.1 Heliocentric transfer phase

As a Sun-driven lunar swingby sequence can reach or absorb a $v_{\infty \text{E}}$ of 1.46 km/s at the least (see Fig. 6), and Δv_{stop} and Δv_{retn} provided by propulsion systems are limited to 1 km/s and 500 m/s, respectively, minimizing the Δv cost in the heliocentric transfer phase is crucial. A Lambert solver for the two-body problem and the Matlab Fmincon routine are used to find low-Δv transfer trajectories between the Earth and asteroids. The free variables, the $\Delta \mathbf{v}$ vector, and epochs of Earth departure, asteroid arrival, asteroid departure, and Earth arrival, are optimized. The Lambert solver can consider multiple revolutions and return multiple solutions. In this work, up to three revolutions of heliocentric transfer are considered. However, the Lambert solver is not called in the optimization routine but is only used to provide initial guesses for $\Delta \mathbf{v}$. Starting with the initial guess, the Fmincon routine can continue to compute the optimal trajectory with the fed gradients whose expressions are available in Ref. [33], p. 467. Furthermore, using the numerical optimization routine for solving the two-point boundary problem can avoid the singularity

problem in the Lambert solver when the revolution number jumps. Once an optimal transfer trajectory with $\Delta v_{\text{stop}} < 1$ km/s (or $\Delta v_{\text{retn}} < 500$ m/s) is found, the corresponding escape (or incident) condition, $\mathbf{v}_{\infty \text{E}}$ as well as its declination δ, is known, and the accessible domain described in Sec. 3.2 can be applied to exclude impossible transfer trajectories.

4.2 Escape and capture phases

The escape (or capture) phase involves a sequence of Moon-to-Moon transfers and lunar swingbys to reduce the initial (or final) $v_{\infty \text{M}}$ to < 800 m/s (or 450 m/s), given the targeted escape (or incident) $\mathbf{v}_{\infty \text{E}}$ connected with the heliocentric transfer phase. In addition, the number of SPMT segments is preferred to be minimal, not only to limit the total flight time but also to minimize the operational risk. The number of SPMT segments is limited to 2 in this work.

Given an escape (or incident) $\mathbf{v}_{\infty \text{E}}$, different lunar encounter positions result in different $\mathbf{v}_{\infty \text{M}}$ (see Appendix) and thus affect the sequence of lunar swingbys. The first (or final) lunar encounter position depends on the phase angle θ (i.e., defined by the angle of the Earth-to-Moon direction from the Sun-to-Earth direction in this work). Strictly speaking, θ depends on the departure (or arrival) date and the ephemeris of the Moon. However, as the ToF of the heliocentric phase (i.e., 250 to 1500 days) is much longer than the synodic period of the Moon (i.e., 30 days), it is assumed that a small Δv can vary the departure (or arrival) date by 15 days without significantly affecting $\mathbf{v}_{\infty \text{E}}$. Therefore, θ is considered to be a variable in the exploration of lunar swingby sequences. This will allow for more options for lunar swingby sequences as well as a higher chance of meeting the $v_{\infty \text{M}}$ objective. To facilitate patching SPMT segments and lunar swingbys, a database of SPMT solutions is used. The following subsection presents the steps for generating this database.

4.2.1 Database of Sun-perturbed Moon-to-Moon Transfers

With significant solar perturbations, the Sun-perturbed Moon-to-Moon Transfer (SPMT) cannot be solved analytically. Nevertheless, the condition of SPMT can be defined by only two variables: θ and $v_{\infty \text{M}}$, which are practically bounded. $v_{\infty \text{M}}$ is bounded as the ToF of an M-M transfer is limited to an acceptable time. Therefore, the grid search method is applicable. The solution of SMPT includes two variables: the post-swingby direction angle ψ of the post-swingby $\mathbf{v}^{+}_{\infty \text{M}}$, and the ToF for a lunar re-encounter. Lantoine and McElrath (2014) [34] classified the SMPT into families according to the ToF range and whether the beginning and the end of the transfer trajectory go in (i.e., noted by "i") or out (i.e.,

noted by "o") of the Moon's orbit. M-M transfers in the same family exhibit a continuation on θ, $v_{\infty \mathrm{M}}$, ψ, and ToF. Therefore, solutions of a family can be recovered if one solution of the family has been obtained. Furthermore, Garcia Yárnoz et al. (2016) [6] used the analytical expression of the gradient of the solution space to generate initial guesses for the neighboring grid nodes. However, they also noted that as ToF increases, the classification of families becomes complicated. Moreover, singularity happens as the perigee of the solution reaches a small value. Thus, it is tricky to determine the profile of families in the solution space. Without full knowledge, the continuation method is likely to miss solutions.

Considering that the database of SPMT, once established, can be accessed repeatedly, efforts and time to establish such a database are not the primary concern. Therefore, despite its tediousness, the following effort has been made to ensure completeness of the database. Solutions for every grid node defined by θ and $v_{\infty \mathrm{M}}$ are computed regardless of the classification of the family. However, there are infinite solutions if ToF is not limited. In this work, ToF is limited to 200 days. In addition, when $v_{\infty \mathrm{M}}$ is smaller than 0.4 km/s, the gravity loss becomes significant and the model of patching M-M transfers in the SE-CR3BP cannot hold very true. When $v_{\infty \mathrm{M}}$ is greater than 2.2 km/s, the trajectory is mostly hyperbolic and cannot come back to the Moon within 200 days. Therefore, a mesh grid is generated by sampling $v_{\infty \mathrm{M}}$ from 0.4 to 2.2 km/s spaced in intervals of 0.1 km/s and θ from 0° to 360° spaced in intervals of 2°. To solve for the SPMT for a given grid node, a combination of adaptable-step searches on ψ and differential correction on ψ and ToF is used (see Ref.[26] for more detail). The constraint that the perigee must be greater than 6600 km for the transfer trajectories is applied. In addition, multiple-revolution (multi-rev) transfers can also be computed with this method. Figure 7 presents example SPMT with an initial $v_{\infty \mathrm{M}} = 1.2\ \mathrm{km/s}$. They are grouped into the families defined by Lantoine and McElrath (2014) [34], where the resonance $p : q$ indicates that the transfer trajectory makes p revolutions (i.e., defined by the number of apogees) while the Moon rotates q revolutions. Changes in lunar encounter situations at the ends of the Sun-perturbed transfers can be clearly seen.

The solution space where the SPMT encounters the Moon tangentially and where ToF is long is highly nonlinear, and therefore the computation is very sensitive to the initial guess. There are solutions missed in the previous step. Thus, in the second step, a scan is performed. To be specific, the continuation method is used to generate solutions for neighboring grid nodes based on every existent solution. When a new solution is found, it is added to the database. With all these efforts, the computed database is believed to be almost complete.

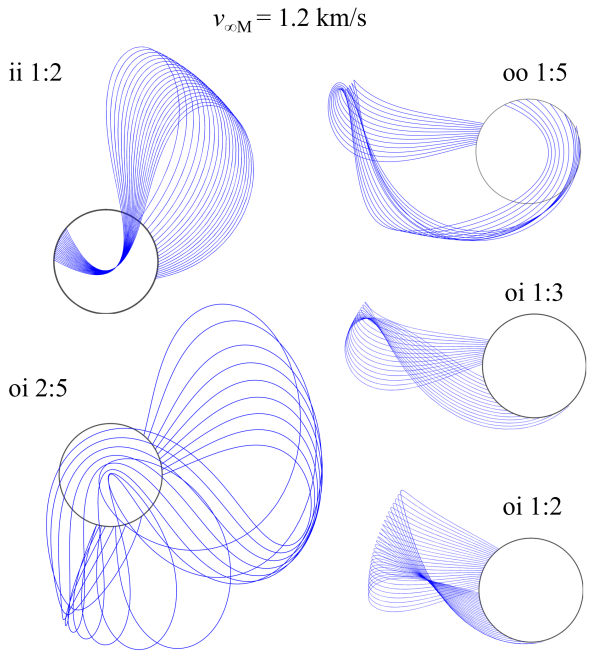

Fig. 7 Examples of Sun-perturbed Moon-to-Moon transfers (synodic frame).

5 Results

Figure 8 summarizes the workflow for finding retrievable asteroids and possible mission and trajectory profiles, where filters defined by the reachable sets, namely, the accessible Jacobi range and $\mathbf{v}_{\infty E}$ domain, are applied. The workflow for asteroid rendezvous is similar to that in Fig. 8 and thus is not presented. Some of the candidates enclosed by the accessible Jacobi range may be found inaccessible for a given interval (e.g., 2023-2043 used in this work) because of unachievable escape (or incident) conditions, or no sequence of lunar swingbys found to meet the initial (or final) $v_{\infty M}$ requirements. Nevertheless, a number of accessible asteroids and feasible mission options are identified.

Table 2 summarizes the 48 asteroids that spacecraft can rendezvous with before 2043. Each asteroid can be reached with a Sun-driven lunar swingby sequence and $\Delta v_{\text{stop}} < 1$ km/s. The orbital elements, the number of observations n_{obs}, number of oppositions, n_{opp}, absolute magnitude, H, suspected diameter, D, and orbit class of the asteroids are also listed for reference of mission planners. Note that for each listed asteroid, there are one to hundreds of heliocentric transfer options whose escape conditions can be met by at least one option of the Sun-driven lunar swingby sequence. Not all feasible mission profiles can be presented in this paper, but options prioritizing the flight time TOF and the asteroid observation time T_{obs} are selected and presented in Table 3. T_{obs} represents the minimum period of observing the asteroid

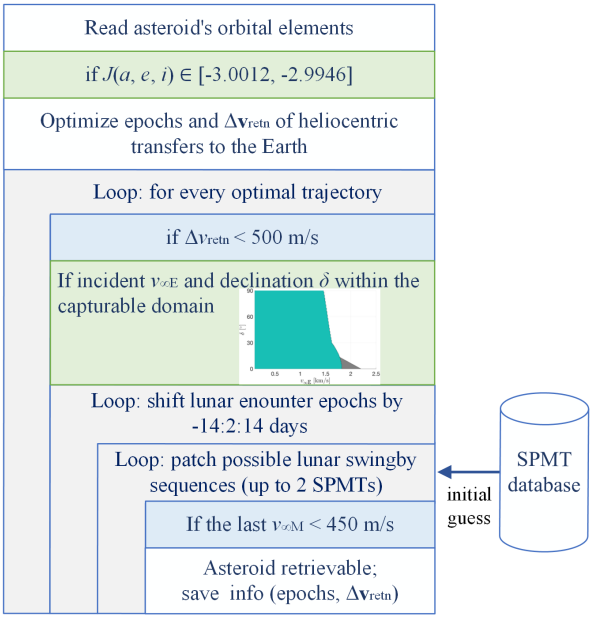

Fig. 8 Workflow for finding retrievable asteroids and feasible trajectory options considering the capacity of a Sun-driven lunar swingby sequence (green blocks).

in case the required Δv_{stop} cannot be fully paid. It is related to H, the velocity vector of the spacecraft with respect to the asteroid, and the camera detection magnitude [35]. Herein, a camera magnitude of 12 is adopted, which was used by the low-cost micro-probe PROCYON [36]. As the table indicates, even without Δv_{stop}, the Sun-driven lunar swingby sequence can still permit asteroid flybys for closely observing asteroids over hours to more than one week (e.g., for 1991 VG, 2000 SG344, 2014 YD, 2017 TB18, and 2017 BN93).

Table 2 Easily reachable asteroids before 2043

Asteroid Des. ID	H	i [°]	e	a [AU]	D [m]	n_{obs}	n_{opp}	Class
1991 VG	28.3	1.4	0.052	1.032	10	66	3	Apollo
2000 LG6	29.0	2.8	0.111	0.917	7	13	1	Aten
2000 SG344	24.7	0.1	0.067	0.977	37	31	2	Aten
2001 GP2	26.4	1.3	0.072	1.035	25	58	2	Apollo
2005 QP87	27.7	0.3	0.175	1.233	10-15	85	1	Amor
2006 RH120	29.5	0.6	0.024	1.033	6	133	2	Apollo
2006 UB17	26.3	2.0	0.103	1.140	15-33	28	1	Amor
2007 UN12	28.7	0.2	0.059	1.049	9	132	2	Apollo

2007 VU6	26.5	1.2	0.091	0.976	13-29	38	1	Aten
2008 EA9	27.7	0.4	0.075	1.050	14	56	1	Apollo
2008 HU4	28.3	1.4	0.056	1.071	7	77	2	Amor
2008 UA202	29.4	0.3	0.068	1.033	5	16	1	Apollo
2009 BD	28.1	1.3	0.051	1.062	10	178	3	Apollo
2009 YR	28.0	0.7	0.110	0.942	12	29	1	Aten
2010 JW34	28.1	2.3	0.055	0.981	12	55	1	Aten
2010 UJ	26.2	0.4	0.092	0.950	20	12	1	Aten
2010 UE51	28.3	0.6	0.060	1.055	7	175	1	Apollo
2010 VQ98	28.2	1.5	0.027	1.023	11	49	1	Apollo
2011 BL45	27.1	3.1	0.021	1.038	18	24	1	Apollo
2011 BQ50	28.0	0.4	0.098	0.950	7-15	25	1	Amor
2011 MD	28.0	2.5	0.037	1.056	5.19	1487	1	Amor/Apollo
2011 UD21	28.5	1.1	0.030	0.979	10	83	1	Aten
2012 TF79	27.4	1.0	0.038	1.050	16	63	1	Apollo
2012 WR10	28.7	0.3	0.112	1.085	9	42	1	Apollo
2013 BS45	25.9	0.8	0.084	0.992	31	92	2	Aten
2013 EC20	29.0	1.3	0.121	1.113	7	55	1	Apollo
2013 RZ53	31.1	2.1	0.028	1.017	2	31	1	Apollo
2014 DJ80	26.3	3.0	0.067	0.977	27	30	1	Aten
2014 HN2	26.3	1.2	0.118	0.927	26	65	1	Aten
2014 QN266	26.3	0.5	0.092	1.053	27	82	1	Apollo
2014 UV210	26.9	0.6	0.132	1.155	20	62	2	Apollo
2014 WU200	29.1	1.3	0.071	1.028	7	46	1	Apollo
2014 WX202	29.6	0.4	0.059	1.036	6	41	1	Apollo
2014 WA366	26.9	1.6	0.071	1.034	20	54	1	Apollo
2014 YD	24.3	1.7	0.087	1.072	20	104	1	Apollo
2015 JD3	25.5	2.7	0.008	1.058	38	37	1	Amor
2015 PS228	28.8	0.4	0.084	1.057	9	38	1	Apollo
2015 VC2	27.4	0.9	0.074	1.053	16	111	2	Apollo
2015 XZ378	27.2	2.7	0.035	1.015	17	35	1	Apollo

2015 YO10	26.6	2.4	0.100	1.122	23	28	1	Apollo
2016 CF137	25.6	2.5	0.100	1.091	36	50	1	Apollo
2016 RD34	27.7	2.0	0.035	1.046	14	90	1	Apollo
2016 TB18	24.8	1.5	0.084	1.077	52	98	1	Apollo
2016 TB57	26.1	0.3	0.123	1.102	29	137	1	Apollo
2017 BN93	25.4	2.1	0.052	1.044	40	15	1	Apollo
2017 FJ3	29.9	1.0	0.118	1.133	5	15	1	Apollo
2017 FT102	29.5	1.5	0.059	1.038	6	79	1	Apollo
2017 HU49	26.5	2.6	0.055	0.971	24	147	1	Aten

Table 3 Selected asteroid flyby and rendezvous missions before 2043 prioritizing flight time and observation time

Asteroid Des. ID	Escape from Earth	Arrival at asteroid	ToF [day]	T_{obs} [day]	Δv_{stop} [m/s]
1991 VG	2038 NOV 29	2041 FEB 23	817	7.9	120.1
2000 LG6	2028 MAY 16	2030 MAY 10	724	0.2	936.9
2000 SG344	2028 MAY 09	2029 JUL 02	418	54.8	44.0
	2028 MAY 10	2030 JUN 20	771	59.2	39.8
2001 GP2	2038 MAR 25	2039 JUL 14	476	1.5	694.2
2005 QP87	2034 AUG 24	2037 JAN 19	879	0.7	770.9
2006 RH120	2028 NOV 14	2029 OCT 01	320	1.5	662.7
2006 UB17	2033 OCT 24	2035 OCT 14	719	1.1	891.0
2007 UN12	2035 OCT 15	2037 NOV 04	752	2.9	138.1
2007 VU6	2037 DEC 15	2039 MAR 01	441	1.0	920.2
2008 EA9	2033 NOV 25	2035 MAR 15	475	2.9	217.8
2008 HU4	2026 APR 25	2027 JUL 29	460	2.3	186.8
	2026 APR 25	2028 OCT 04	893	3.5	94.1
2008 UA202	2028 OCT 20	2030 SEP 22	702	1.3	209.2
2009 BD	2034 JUN 03	2035 MAY 07	338	1.8	258.3
2009 YR	2031 NOV 15	2033 APR 05	507	1.5	535.4
2010 JW34	2039 NOV 05	2042 JUL 27	995	1.1	887.1
2010 UJ	2034 SEP 19	2035 MAY 25	248	3.5	369.9

2010 UE51	2036 NOV 25	2037 OCT 11	320	2.6	390.0
2010 VQ98	2039 NOV 13	2041 OCT 01	688	4.3	198.7
	2039 NOV 08	2042 SEP 05	1032	5.1	87.2
2011 BL45	2028 AUG 15	2029 JUL 01	320	0.8	751.3
2011 BQ50	2037 FEB 02	2038 MAR 09	400	0.8	663.0
2011 MD	2036 JUN 23	2038 SEP 10	809	3.7	134.4
2011 UD21	2039 APR 14	2041 JAN 14	641	0.7	589.8
2012 TF79	2026 APR 09	2027 DEC 01	601	1.7	375.5
	2027 FEB 14	2028 DEC 20	675	1.8	862.8
2012 WR10	2038 OCT 13	2039 MAR 18	156	1.4	667.8
2013 BS45	2024 NOV 15	2026 MAY 16	547	1.5	977.2
2013 EC20	2033 MAY 15	2035 JUN 10	756	0.1	983.0
2013 RZ53	2023 SEP 06	2027 NOV 28	1544	0.3	484.7
2014 DJ80	2038 AUG 14	2040 MAY 04	629	0.9	993.0
2014 HN2	2029 MAR 06	2032 MAR 11	1101	1.3	772.6
2014 QN266	2026 FEB 14	2027 MAY 05	445	1.4	820.8
2014 UV210	2034 NOV 14	2036 MAR 14	486	1.1	783.1
2014 WU200	2039 DEC 17	2040 SEP 17	275	2.8	104.7
2014 WX202	2035 FEB 13	2036 JAN 04	325	1.3	406.0
	2034 NOV 28	2037 MAR 15	838	2.4	100.6
2014 WA366	2033 NOV 28	2034 SEP 25	301	1.3	650.8
2014 YD	2035 APR 30	2036 FEB 25	301	3.1	967.8
	2024 JAN 18	2027 MAY 25	1223	8.2	348.3
2015 JD3	2039 MAY 04	2040 DEC 24	600	5.3	663.1
2015 PS228	2027 AUG 16	2028 JUN 06	295	0.7	475.0
2015 VC2	2029 MAR 19	2031 JAN 01	653	3.8	188.9
2015 XZ378	2023 MAY 17	2026 OCT 26	1258	0.7	865.3
2015 YO10	2028 JAN 18	2028 NOV 18	306	0.9	957.5
2016 CF137	2040 JAN 31	2040 DEC 02	306	1.9	776.0
2016 RD34	2031 SEP 12	2033 AUG 11	699	6.2	87.4

2016 TB18	2026 MAR 29	2027 FEB 01	309	6.8	309.4
2016 TB57	2024 JAN 20	2025 JAN 21	367	2.3	542.5
2017 BN93	2032 AUG 14	2033 NOV 21	464	7.2	725.4
2017 FJ3	2034 MAR 04	2035 JUN 02	455	0.3	831.3
2017 FT102	2034 SEP 29	2035 JUN 13	257	0.3	863.0
2017 HU49	2039 MAY 15	2040 MAR 05	295	3.6	669.4

Regarding asteroid sample return and retrieval, 25 targets are found to be possible by 2043. Each can be retrieved with a Sun-driven lunar swingby sequence and a $\Delta v_{\text{retn}} < 500$ m/s. Again, not all feasible mission profiles can be presented, but the representative missions prioritizing Δv_{retn} are presented in Table 5. Readers interested in all mission options may contact the author. All retrievable targets are included in the list of easily reachable asteroids, and thus readers can refer to Table 2 for general information on these targets. Among the listed missions, Δv_{retn} is particularly small for the 1991 VG mission, which is 32 m/s. Even though 1991 VG is 5 to 10 times heavier than 2006 RH120 and 2008 UA202, the required total impulse to return 1991 VG to the vicinity of the Earth is still the lowest of all listed missions. The mass of 1991 VG, which measures 10 m across, is estimated to be 1500 tons (i.e., at an assumed density of 2.8 g/cm^3). The required total impulse is 4.6×10^4 kN $\cdot$ s, which is within the capacity of state-of-the-art heavy-lift boosters [15].

If a low-cost asteroid rendezvous is also required, Table 5 presents representative low-cost retrieval missions for 16 asteroids, prioritizing the total flight time ToF_{tot} in the heliocentric phase. To exemplify, Fig. 9 presents a set of trajectory options for the 1991 VG retrieval mission, and Fig. 10 presents the trajectory options for a 2000 SG344 sample-return mission.

6 Discussions

6.1 Considerations and applications of transfer options

Figure 11 presents options of gravity-assisted trajectories for capturing the sample from 2009 BD arriving in the vicinity of the Earth around 2033 May 15. The upper-left panel demonstrates the capture trajectory adopting a short inner M-M transfer and two Sun-perturbed transfers. The upper-right panel demonstrates another option adopting a three-rev transfer. The inner M-M transfer is not always necessary. Furthermore, it is considered not very practical for the challenging GNC operation to be performed within the short

Table 4 Selected asteroid sample-return and retrieval missions prioritizing Δv_{retn}

Asteroid	Departure for Earth	Arrival at Earth	Δv_{retn} [m/s]
1991 VG	2036 JAN 07	2038 DEC 03	31.6
2000 SG344	2028 MAR 13	2030 OCT 07	182.9
2006 RH120	2028 APR 13	2028 NOV 12	143.6
2007 UN12	2031 NOV 09	2035 OCT 26	75.8
2008 EA9	2030 FEB 11	2034 FEB 08	70.0
2008 HU4	2033 FEB 22	2037 APR 25	148.7
2008 UA202	2025 DEC 02	2028 OCT 05	161.8
2009 BD	2031 APR 22	2035 JUN 04	142.6
2010 JW34	2038 JUN 03	2041 MAY 10	396.5
2010 UJ	2032 MAY 09	2033 DEC 06	389.6
2010 UE51	2035 JUN 08	2036 NOV 06	131.9
2010 VQ98	2039 FEB 06	2040 NOV 06	65.4
2011 UD21	2038 JUL 25	2041 OCT 11	68.0
2012 TF79	2026 MAR 03	2027 OCT 14	346.4
2014 WU200	2035 JUN 22	2038 DEC 18	104.0
2014 WX202	2030 JUL 26	2033 NOV 24	94.5
2014 WA366	2030 APR 23	2034 JUL 07	489.7
2014 YD	2034 JAN 21	2036 JAN 19	353.2
2015 PS228	2026 APR 23	2029 MAR 11	489.7
2015 VC2	2025 JAN 05	2029 FEB 19	281.2
2016 RD34	2029 SEP 09	2032 SEP 12	151.6
2016 TB18	2032 JUL 27	2036 MAR 19	234.4
2017 BN93	2027 AUG 24	2031 AUG 08	166.7
2017 FJ3	2028 MAR 16	2029 MAR 13	479.9
2017 FT102	2030 SEP 09	2034 APR 19	485.4

period between two consecutive lunar swingbys. As for multi-rev M-M transfers, as they regularly pass the orbit of the Moon, they can be perturbed by the gravity of the Moon, which is not described by the “simplified" model used in this work. Hence, the designed trajectory involving multi-rev M-M transfers cannot be used directly without further refinement in the high-fidelity model. Nevertheless, this simplified model provides insights into orbit dynamics and handy approaches to orbit design, which are tricky to achieve in a high-fidelity model. A number of transfer options generated by this method can serve as the

Table 5 Selected asteroid sample-return and retrieval missions constrained by gravity-assisted asteroid rendezvous and prioritizing the total flight time

Asteroid	Escape from Earth	Arrival at asteroid	Δv_{stop} [m/s]	Departure for Earth	Δv_{retn} [m/s]	Return to Earth	ToF_{tot} [day]
1991 VG	2031 NOV 29	2035 SEP 18	949	2036 JAN 07	31.6	2038 DEC 03	2561
2000 SG344	2024 FEB 15	2026 JUL 03	730	2027 NOV 07	221.2	2029 APR 06	1877
2006 RH120	2024 JAN 27	2026 OCT 11	828	2027 JUL 08	438.6	2028 OCT 23	1731
2007 UN12	2030 FEB 14	2033 AUG 22	973	2033 SEP 26	149.0	2035 OCT 19	2073
2008 HU4	2024 FEB 15	2027 JUN 22	978	2033 FEB 17	335.6	2036 APR 28	4456
2008 UA202	2024 FEB 15	2026 AUG 04	918	2026 DEC 21	329.2	2028 OCT 05	1694
2009 BD	2024 MAY 16	2026 OCT 14	712	2029 JAN 03	418.2	2033 MAY 23	3294
2010 UJ	2024 OCT 20	2028 JAN 18	638	2029 JUL 29	410.2	2032 DEC 04	2967
2010 UE51	2024 NOV 15	2027 APR 04	784	2031 SEP 04	470.4	2035 NOV 27	4029
2010 VQ98	2029 NOV 14	2033 JUL 20	961	2034 SEP 26	471.9	2037 OCT 29	2905
2011 UD21	2031 APR 17	2035 APR 21	884	2035 NOV 17	398.2	2038 OCT 15	2738
2014 WU200	2031 JUN 18	2035 JAN 03	942	2035 JUN 22	104.0	2038 DEC 18	2740
2012 TF79	2024 FEB 15	2026 DEC 03	839	2039 JAN 27	397.9	2042 OCT 18	6820
2014 WX202	2027 MAY 17	2030 DEC 07	991	2032 SEP 27	273.9	2033 NOV 23	2382
2015 VC2	2025 MAR 27	2029 JAN 14	807	2037 NOV 01	473.5	2041 DEC 31	6123
2016 TB18	2024 MAR 30	2028 APR 09	570	2034 DEC 05	273.1	2036 MAR 24	4377

initial guesses for orbit optimization in a high-fidelity model. The trajectory refinement and optimization may result in a few small Δv during the courses of the M-M transfers, which is to either avoid or to make use of the gravity of the Moon. Lantoine and McElrath (2014) [34] have demonstrated that the Sun-driven lunar swingby sequence designed in this simplified model can be successfully transferred to the ephemeris model without significant correction.

In addition, options without a short inner transfer or multi-rev transfer may be available. The bottom two panels present the trajectory options for different first lunar phase angles (or the Earth encounter dates). In the bottom-left panel, the retrograde transfer arc is greatly altered around the apogee in the 2nd quadrant, and the orbit finally becomes a posigrade orbit with a small $v_{\infty \text{M}}$. However, the two SPMTs take as long as 200 days. The bottom-right panel demonstrates a more favorable option, where only one large M-M transfer arc and one lunar swingby are needed, which results in a minimum flight time (i.e., 120 days) and GNC challenge. To summarize, it is advantageous to have a complete database of SPMT (e.g., including multi-rev transfers) and fully explore all possible sequences, so as to gain flexibility and

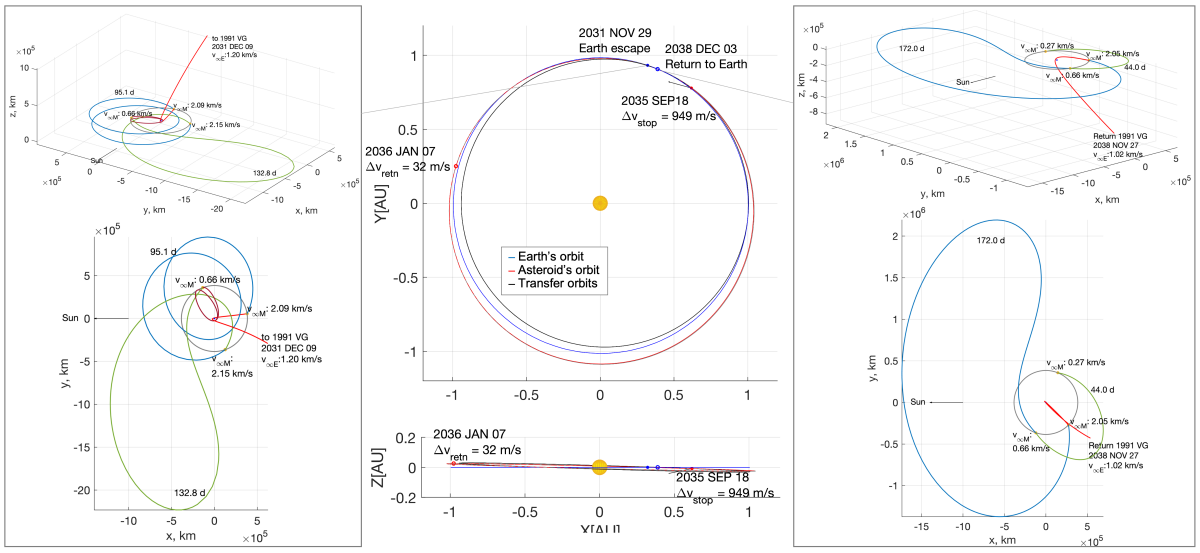

Fig. 9 An example mission profile for 1991 VG retrieval, with a gravity-assisted escape phase (left), a heliocentric transfer phase for the asteroid rendezvous and Earth re-encounter (middle), and a gravity-assisted capture phase (right).

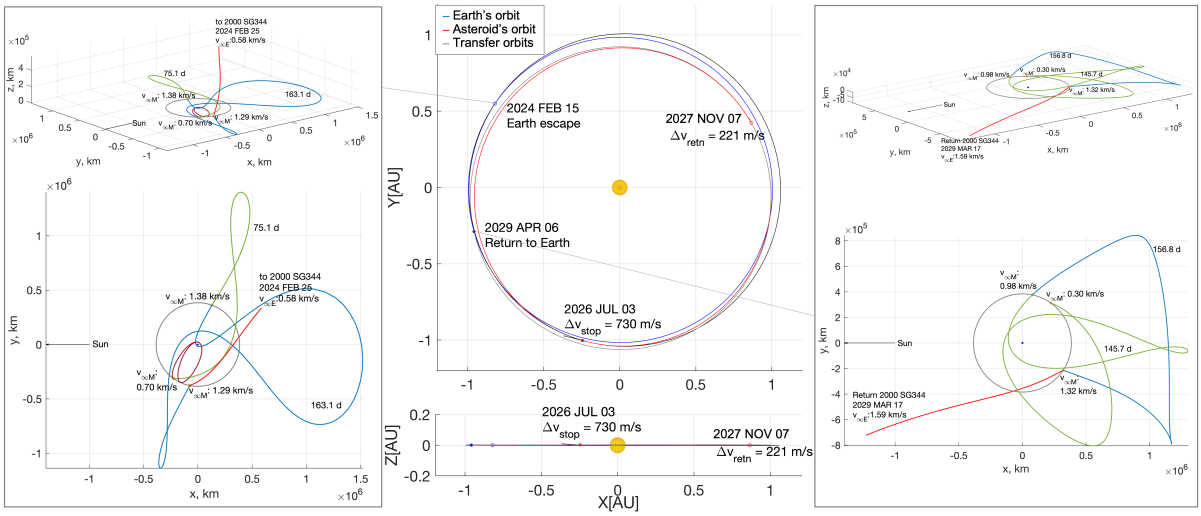

Fig. 10 An example mission profile for 2000 SG344 sample return, with a gravity-assisted escape phase (left), a heliocentric transfer phase for the asteroid rendezvous and Earth re-encounter (middle), and a gravity-assisted capture phase (right).

robustness with backup options.

6.2 Three-dimensional Moon-to-Moon transfers

The three-dimensional (3D) SPMT also exists and can serve to connect two lunar encounters. A database of 3D transfers has also been computed using a similar routine to that presented in Sec. 4.2.1. Example

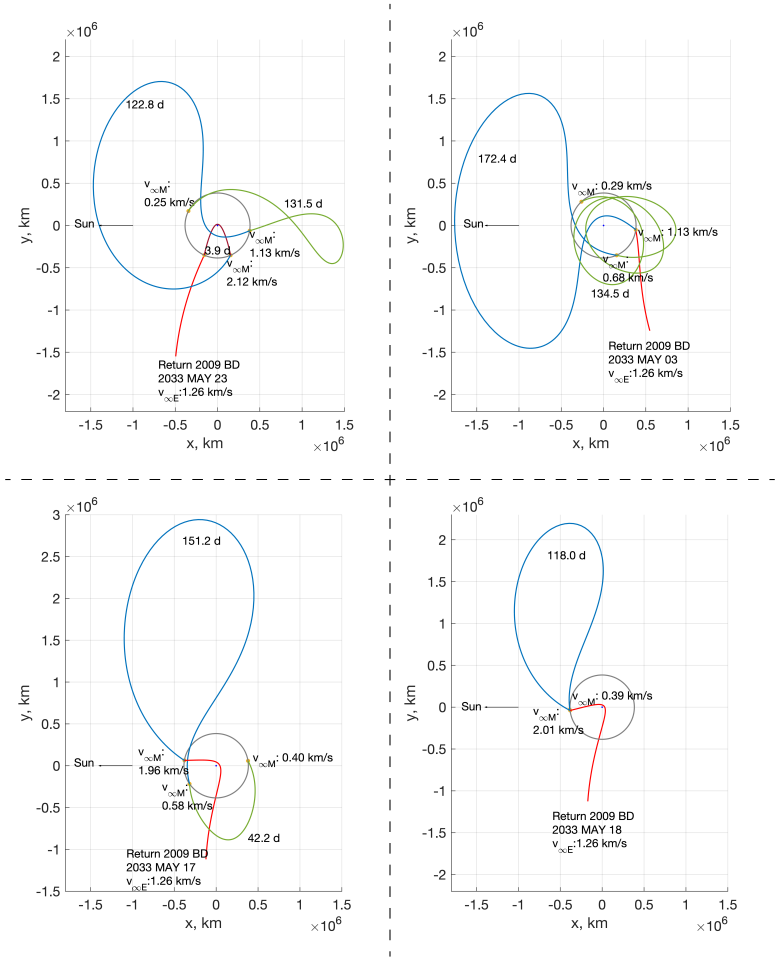

Fig. 11 Available options of lunar swingby sequence for capturing the 2009 BD sample arriving around 2033 May 15 (synodic frame).

3D trajectories (i.e., $v_{\infty \mathrm{M}} = 1.2$ km/s; "oo 1:2" family) are shown in Fig.12. Observation of the 3D solutions shows that $v_{\infty \mathrm{M}}$ at the lunar encounters are generally large (i.e., > 0.8 km/s). That is because the out-of-plane component of $\mathbf{v}_{\infty \mathrm{M}}$ cannot be significantly varied by solar tides. A 3D transfer can change the connecting phase, similar to what a non-perturbed lunar resonant orbit can do, and thus add more patching options. Nevertheless, this is considered not efficient especially for the considered problem, in which ToF and segments of perturbed M-M transfers are limited. Therefore, for the escape phase, it is preferred to perform a sequence of planar M-M transfers and lunar swingbys before the final bend to the out-of-plane trajectory heading for the asteroid. Similarly, for the capture phase, it is preferred to first bend the out-of-plane incident trajectory onto the plane for the following effective gravity assists performed in the plane.

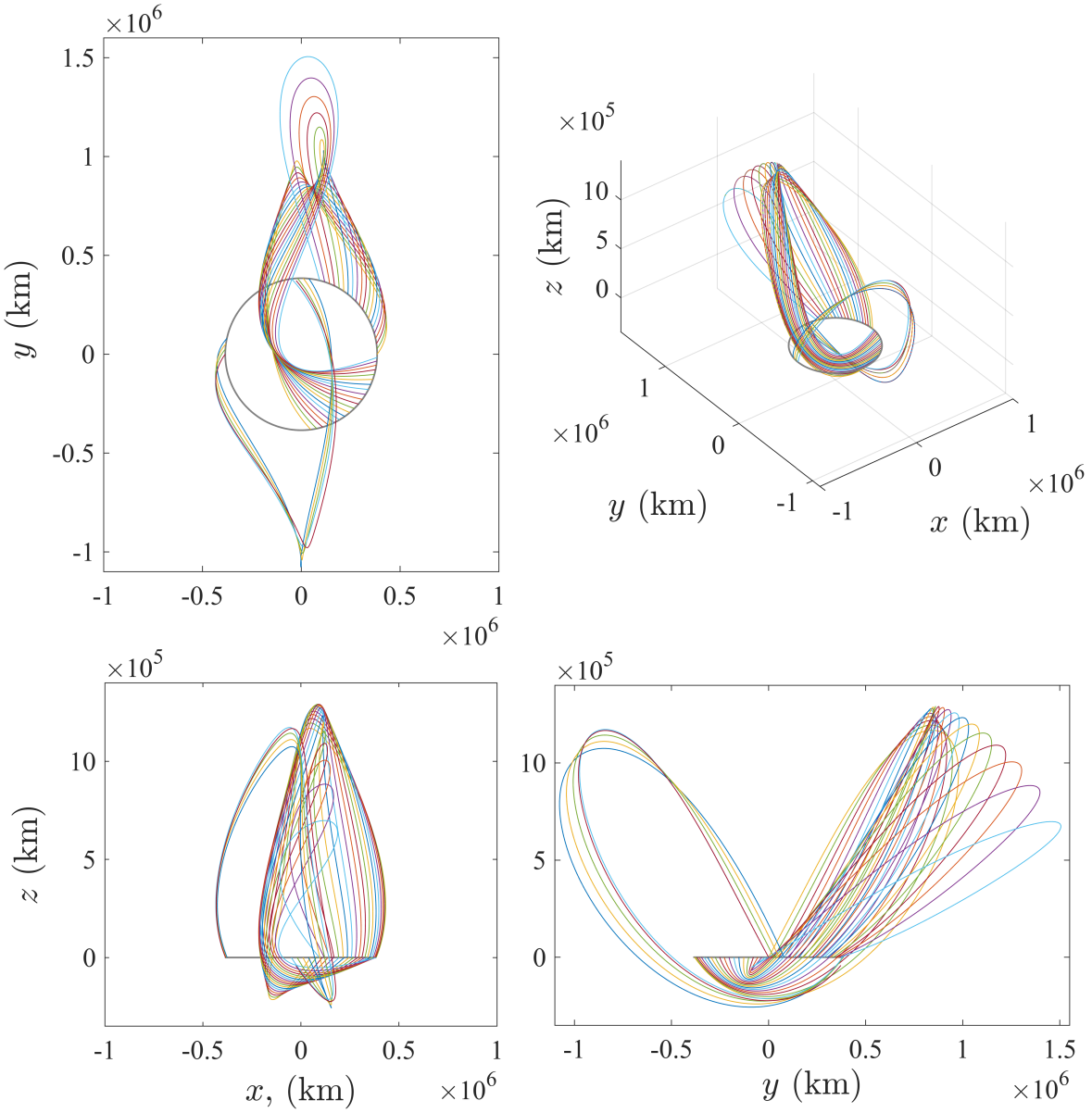

Fig. 12 Example three-dimensional Sun perturbed Moon-to-Moon transfers (synodic frame).

7 Conclusions

The capacity and application of the Sun-driven lunar swingby sequence are presented in this paper. A variety of types of Moon-to-Moon transfers, namely, the short transfer, Sun-perturbed transfer, multi-rev transfer, and three-dimensional transfer, were discussed. Analyses with the "Swingby-Jacobi" graph indicate that

(1) A Sun-driven lunar swingby sequence can access a range of the Jacobi integral from -3.0009 to -2.9946. This range encloses 657 potential asteroids currently cataloged, which can reduce the

effort of target search and trajectory optimization.

(2) C_3 for escape can be increased to 4.8 km^2/s^2. Reversely, objects of this C_3 level can possibly (depending on the direction) be captured. In particular, this technique can at least reach or absorb a $v_{\infty \mathrm{E}}$ of 1.46 km/s (i.e., C_3 of 2.13 km^2/s^2) in all directions.

Heliocentric transfer trajectories between the Earth and potential candidates were optimized, and massive sequences of lunar swingbys were explored thanks to the database of Sun-perturbed Moon-to-Moon transfers. Results show that Sun-driven lunar swingby sequences can enable:

(3) spacecraft to rendezvous with 48 asteroids by 2043, at a Δv cost of less than 1 km/s after the first lunar encounter. Even without the rendezvous Δv, spacecraft can still flyby and observe the asteroids such as 1991 VG, 2000 SG344, 2014 YD, 2016 TB18, and 2017 BN93 for more than one week. This is still significant for a low-cost mission.

(4) 25 asteroid samples to be captured by 2043, at a Δv cost of less than 500 m/s for the Earth re-encounter (while lunar orbit injection requires an additional 20 to 350 m/s of Δv). In particular, given the capabilities of state-of-the-art launch and propulsion systems, retrieving the entire 10-m asteroid 1991 VG in 2038, which requires a total impulse of 4.6×10^4 kN $\cdot$ s, is considered feasible.

Appendix (Patching the heliocentric phase and the lunar swingby sequence)

Considering the capture case, given the incident $\mathbf{v}_{\infty \mathrm{E}}$ and the Moon's position vector $\mathbf{r}_{\mathrm{M}}$ as the encounter conditions, the orbital elements of the hyperbolic orbit about Earth can be computed with the routine presented in this appendix. There are two situations of encounters. One kind of encounter takes place on the inbound leg, and another kind of encounter takes place on the outbound leg (see Fig.13). For the inbound-capture case, the relationship between the true anomaly f at the encounter, turn angle ζ (i.e., half the bending angle), and the angle β between $\mathbf{v}_{\infty \mathrm{E}}$ and $\mathbf{r}_{\mathrm{M}}$ is expressed by:

$$\cos f = \cos(\beta - \zeta) \tag{13}$$

which can be rewritten as:

$$\cos f = \sin\beta \sin\zeta + \cos\beta \cos\zeta \tag{14}$$

ζ is related to the eccentricity e_{p} of the orbit about Earth. The subscript "p" indicates the orbit about the planet. Hence,

$$\cos f = \frac{\sqrt{e_{\mathrm{p}}^2 - 1}}{e_{\mathrm{p}}} \sin\beta + \frac{1}{e_{\mathrm{p}}} \cos\beta \tag{15}$$

At the encounter, the radius of the hyperbolic orbit is the same as the radius of Moon's orbit, which is expressed as:

$$r_{\mathrm{M}} = \frac{a_{\mathrm{p}}(1-e_{\mathrm{p}}^2)}{1+e_{\mathrm{p}}\cos f} \tag{16}$$

where the semi-major axis a_{p} is related to $v_{\infty \mathrm{E}}$ through,

$$a_{\mathrm{p}} = -G_{\mathrm{E}}/v_{\infty \mathrm{E}}^2 \tag{17}$$

where G_{E} is the gravitational parameter of the Earth. Integrating the last two equations yields a quadratic function of $\sqrt{e_{\mathrm{p}}^2-1}$,

$$a_{\mathrm{p}}(e_{\mathrm{p}}^2-1) + r_{\mathrm{M}}\sin\beta\sqrt{e_{\mathrm{p}}^2-1} + r_{\mathrm{M}}(1+\cos\beta) = 0 \tag{18}$$

whose solution is computed from,

$$\sqrt{e_{\mathrm{p}}^2-1} = \frac{-r_{\mathrm{M}}\sin\beta - \sqrt{r_{\mathrm{M}}^2\sin^2\beta - 4a_{\mathrm{p}}r_{\mathrm{M}}(1+\cos\beta)}}{2a_{\mathrm{p}}} \tag{19}$$

With e_{p} known, the orbit can be determined. The true anomaly is computed from:

$$f = -\arccos\left[\frac{a_{\mathrm{p}}(1-e_{\mathrm{p}}^2)-r_{\mathrm{M}}}{r_{\mathrm{M}}e_{\mathrm{p}}}\right] \tag{20}$$

Other desired orbital information at the lunar encounter can be derived. The steps of deriving e_{p} and f for the outbound-capture, inbound-escape, and outbound-capture cases are similar. The corresponding expressions are directly given as follows. For the outbound-capture case:

$$\sqrt{e_{\mathrm{p}}^2-1} = \frac{r_{\mathrm{M}}\sin\beta - \sqrt{r_{\mathrm{M}}^2\sin^2\beta - 4a_{\mathrm{p}}r_{\mathrm{M}}(1+\cos\beta)}}{2a_{\mathrm{p}}} \tag{21}$$

$$f = \arccos\left[\frac{a_{\mathrm{p}}(1-e_{\mathrm{p}}^2)-r_{\mathrm{M}}}{r_{\mathrm{M}}e_{\mathrm{p}}}\right] \tag{22}$$

For the inbound-escape case:

$$\sqrt{e_{\mathrm{p}}^2-1} = \frac{r_{\mathrm{M}}\sin\beta - \sqrt{r_{\mathrm{M}}^2\sin^2\beta - 4a_{\mathrm{p}}r_{\mathrm{M}}(1-\cos\beta)}}{2a_{\mathrm{p}}} \tag{23}$$

$$f = -\arccos\left[\frac{a_{\mathrm{p}}(1-e_{\mathrm{p}}^2)-r_{\mathrm{M}}}{r_{\mathrm{M}}e_{\mathrm{p}}}\right] \tag{24}$$

For the outbound-escape case:

$$\sqrt{e_{\mathrm{p}}^2-1} = -\frac{r_{\mathrm{M}}\sin\beta + \sqrt{r_{\mathrm{M}}^2\sin^2\beta - 4a_{\mathrm{p}}r_{\mathrm{M}}(1-\cos\beta)}}{2a_{\mathrm{p}}} \tag{25}$$

$$f = \arccos\left[\frac{a_{\mathrm{p}}(1-e_{\mathrm{p}}^2)-r_{\mathrm{M}}}{r_{\mathrm{M}}e_{\mathrm{p}}}\right] \tag{26}$$

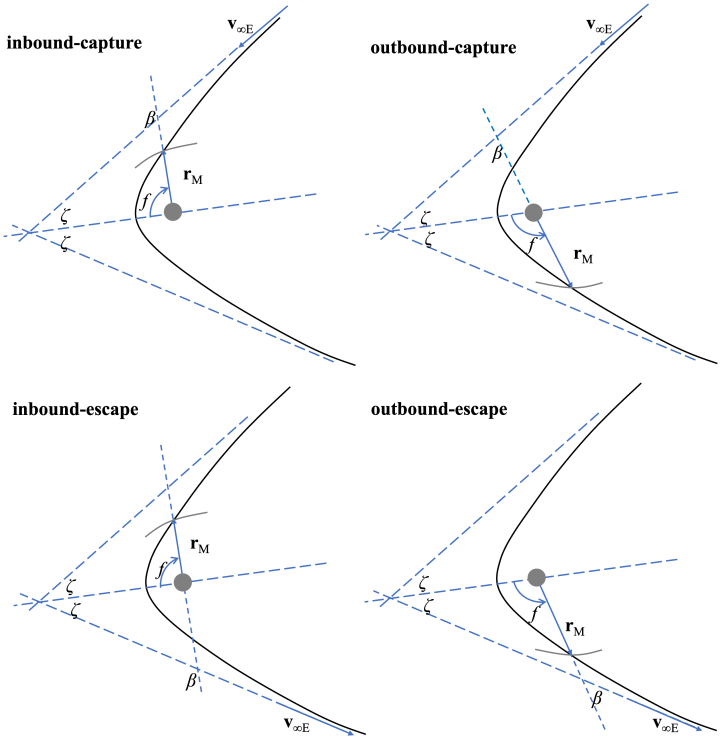

Fig. 13 Situations of lunar encounters with a hyperbolic orbit on the inbound leg and outbound leg.

Acknowledgements

This work was primarily conducted at the Technology and Engineering Center for Space Utilization, Chinese Academy of Sciences. The massive exploration of sequences of Moon-to-Moon transfers and lunar swingbys benefited from the computer cluster `cerfeuil`, financed and managed by IMCCE/Paris Observatory. The author sincerely appreciates the valuable comments from the anonymous reviewers.

Declaration of competing interest

The authors have no competing interests to declare that are relevant to the content of this article.

References

[1] Uesugi K, Matsuo H, Kawaguchi J, Hayashi T. Japanese first double lunar swingby mission “Hiten”. *Acta Astronautica*, 1991, 25(7): 347–355, doi:10.1016/0094-5765(91)90014-V.

[2] Folta DC, Woodard M, Howell K, Patterson C, Schlei W. Applications of multi-body dynamical environments: The ARTEMIS transfer trajectory design. *Acta Astronautica*, 2012, 73: 237–249, doi:10.1016/j.actaastro.2011.11.007.

[3] Kawaguchi J, Nakatani I, Uesugi T, Tsuruda K. Synthesis of an alternative flight trajectory for Mars explorer, Nozomi. *Acta Astronautica*, 2003, 52(2): 189–195, doi:10.1016/S0094-5765(02)00156-X, selected Proceedings of the 4th IAA International conference on Low Cost Planetary Missions.

[4] Chen H. NEW RESULTS OF ORBITAL DYNAMICS AND THE APPLICATION TO ORBIT PREDICTION AND MISSION DESIGN. Phd thesis, Kyushu University, 2015, doi:10.15017/1543984, 63-157.

[5] Chen H, Kawakatsu Y, Hanada T. Earth Escape from a Sun-Earth Halo Orbit using Unstable Manifold and Lunar Swingbys. *Transactions of the Japan Society for Aeronautical and Space Sciences*, 2016, 59(5): 269–277, doi:10.2322/tjsass.59.269.

[6] Garcia Yárnoz D, Yam CH, Campagnola S, Kawakatsu Y. EXTENDED TISSERAND-POINCARE GRAPH AND MULTIPLE LUNAR SWINGBY DESIGN WITH SUN PERTURBATION. In *6th International Conference on Astrodynamics Tools and Techniques*, Darmastadt, Germany2016.

[7] Grebow D, Campagnola S, Haw R, Sweeter T. Lunar Flashlight Mission Overview. In *Inter-planetary Small Satellite Conference*, Pasadena, CA, USA2020.

[8] Cheng AF, Rivkin AS, Michel P, Atchison J, Barnouin O, Benner L, Chabot NL, Ernst C, Fahnestock EG, Kueppers M, Pravec P, Rainey E, Richardson DC, Stickle AM, Thomas C. AIDA DART asteroid deflection test: Planetary defense and science objectives. *Planetary and Space Science*, 2018, 157: 104–115, doi:10.1016/j.pss.2018.02.015.

[9] Michel P, Küppers M, Bagatin AC, Carry B, Charnoz S, de Leon J, Fitzsimmons A, Gordo P, Green SF, Hérique A, Juzi M, Özgür Karatekin, Kohout T, Lazzarin M, Murdoch N, Okada T, Palomba E, Pravec P, Snodgrass C, Tortora P, Tsiganis K, Ulamec S, Vincent JB, Wünnemann K, Zhang Y, Raducan SD, Dotto E, Chabot N, Cheng AF, Rivkin A, Barnouin O, Ernst C, Stickle A, Richardson DC, Thomas C, Arakawa M, Mioto H, Nakamura A, Sugita S, Yoshikawa M, Abell P, Asphaug E, Ballouz RL, Bottke WF, Lauretta DS, Walsh KJ, Martino P, Carnelli I. The ESA Hera Mission: Detailed Characterization of the DART Impact Outcome and of the Binary Asteroid (65803) Didymos. *The Planetary Science Journal*, 2022, 3(7): 160, doi:10.3847/PSJ/ac6f52.

[10] Brophy JR, Friedman L, Culick F. Asteroid retrieval feasibility. In *Proceedings of 2012 IEEE Aerospace Conference*, Big Sky, MT, USA2012, 1–16, doi:10.1109/AERO.2012.6187031.

[11] Baoyin HX, Chen Y, Li JF. Capturing near earth objects. *Research in Astronomy and Astrophysics*, 2010, 10(6): 587, doi:10.1088/1674-4527/10/6/008.

[12] Sanchez Cuartielles JP, Garcia Yarnoz D, Alessi E, McInnes C. Gravitational capture opportunites

for asteroid retrieval missions. In *Proceedings of 63rd International Astronautical Congress*, Naples, Italy2012.

[13] Lladó N, Ren Y, Masdemont JJ, Gómez G. Capturing small asteroids into a Sun–Earth Lagrangian point. *Acta Astronautica*, 2014, 95: 176–188, doi:10.1016/j.actaastro.2013.11.007.

[14] Sanchez JP, Garcia Yárnoz D. Asteroid retrieval missions enabled by invariant manifold dynamics. *Acta Astronautica*, 2016, doi:10.1016/j.actaastro.2016.05.034.

[15] Landau D, Dankanich J, Strange N, Bellerose J, Llanos P, Tantardini M. Trajectories to NAB a NEA (near-Earth asteroid). *Advances in the Astronautical Sciences*, 2013, 148(February): 3251–3262.

[16] Gong S, Li J. Asteroid capture using lunar flyby. *Advances in Space Research*, 2015, 56(5): 848–858, doi:10.1016/j.asr.2015.05.020.

[17] Urrutxua H, Scheeres DJ, Bombardelli C, Gonzalo JL, Peláez J. Temporarily Captured Asteroids as a Pathway to Affordable Asteroid Retrieval Missions. *Journal of Guidance, Control, and Dynamics*, 2015, 38(11): 2132–2145, doi:10.2514/1.G000885.

[18] Mingotti G, Topputo F, Bernelli-Zazzera F. Optimal low-thrust invariant manifold trajectories via attainable sets. *Journal of Guidance, Control, and Dynamics*, 2011, 34(6): 1644–1655, doi:10.2514/1.52493.

[19] Chilan CM, Conway Ba. A Reachable Set Analysis Method for Generating Near-Optimal Trajectories of Constrained Multiphase Systems. *Journal of Optimization Theory and Applications*, 2014, 167: 161–194, doi:10.1007/s10957-014-0651-2.

[20] Bando M, Scheeres DJ. Attractive Sets to Unstable Orbits Using Optimal Feedback Control. *Journal of Guidance, Control, and Dynamics*, 2016, 39(12): 2725–2739, doi:10.2514/1.G000524.

[21] Topputo F, Wang Y, Giordano C, Franzese V, Goldberg H, Perez-Lissi F, Walker R. Envelop of reachable asteroids by M-ARGO CubeSat. *Advances in Space Research*, 2021, 67(12): 4193–4221, doi:https://doi.org/10.1016/j.asr.2021.02.031.

[22] Wu CY, Russell R. Reachable Set of Low-Delta-v Trajectories Following a Gravity-Assist Flyby. *Journal of Spacecraft and Rockets*, 2023, doi:10.2514/1.A35464, in press.

[23] Strange NJ, Longuski JM. Graphical Method for Gravity-Assist Trajectory Design. *Journal of Spacecraft and Rockets*, 2002, 39(1): 9–16, doi:10.2514/2.3800.

[24] Campagnola S, Russell RP. Endgame Problem Part 2: Multibody Technique and the Tisserand-Poincare Graph. *Journal of Guidance, Control, and Dynamics*, 2010, 33(2): 476–486, doi:10.2514/1.44290.

[25] Ross SD, Scheeres DJ. Multiple Gravity Assists, Capture, and Escape in the Restricted Three-Body Problem. *SIAM Journal on Applied Dynamical Systems*, 2007, 6(3): 576–596, doi: 10.1137/060663374.

[26] Chen H. THE USE OF LUNI-SOLAR GRAVITY ASSISTS FOR ASTEROID RETRIEVAL. In JW McMahon, FW Leve, Y Guo, Jon, editors, *Advances in the Astronautical Sciences*, volume 160, 2017, 4043–4060, also proceddings of the AAS/AIAA Spaceflight Mechanics Meeting, San Antonio, TX, USA, FEB 05-09, 2017.

[27] Martens W, Bucci L. Double Tisserand graphs for low-energy lunar transfer design. *Frontiers in Space Technologies*, 2022, 3, doi:10.3389/frspt.2022.920456.

[28] Oguri K, Oshima K, Campagnola S, Kakihara K, Ozaki N, Baresi N, Kawakatsu Y, Funase R. EQUULEUS Trajectory Design. *The Journal of the Astronautical Sciences*, 2020, 67(3): 950–976, doi:10.1007/s40295-019-00206-y.

[29] Thompson M, Kayser E, Parker J, Ott C, Bolliger M, Gardner T, Cheetham B. Navigation Design of the CAPSTONE Mission Near NRHO Insertion. In *AAS/AIAA Astrodynamics Specialist Conference*, Big Sky, MT, USA2021.

[30] Curtis HD. Chapter 8 - Interplanetary Trajectories. In HD Curtis, editor, *Orbital Mechanics for Engineering Students (Third Edition)*, third edition edition, Boston: Butterworth-Heinemann2014, 405–457, doi:https://doi.org/10.1016/B978-0-08-097747-8.00008-6.

[31] Kemble S. *Interplanetary Mission Analysis and Design*, chapter Special techniques, Berlin, Heidelberg: Springer Berlin Heidelberg2006, 135–333, doi:10.1007/3-540-37645-3_4.

[32] McElrath TP, Lantoine G, Landau D, Grebow D, Strange N, Wilson R, Sims J. Using gravity assists in the Earth-Moon system as a gateway to the solar system. In *Global Space Exploration Conference*, Washington, D. C., USA: Pasadena, CA : JPL, NASA2012.

[33] Battin RH. *An Introduction to the Mathematics and Methods of Astrodynamics*. Rev. ed. edition, Reston, Virigina: American Institute of Aeronautics and Astronautics, Inc.1999, doi:10.2514/4.861543.

[34] Lantoine G, McElrath TP. FAMILIES OF SOLAR-PERTURBED MOON-TO-MOON TRANSFERS. In *AAS/AIAA Space Flight Mechanics Meeting*, Santa Fe, USA2014.

[35] Dymock R. The H and G magnitude system for asteroids. *Journal of the British Astronomical Association*, 2007, 117: 342–343.

[36] Yam C, Sugimoto Y, Ozaki N, Sarli B, Chen H, Campagnola S, Ogura S, Kawabata Y, Kawakatsu

Y, Nakajima S, Funase R, Nakasuka S. Launch window and sensitivity analysis of an asteroid flyby mission with miniature ion propulsion system: PROCYON. In *Proceedings of the International Astronautical Congress, IAC*, volume 8, Toronto, Canada2014, 5383 – 5389.

Author biography

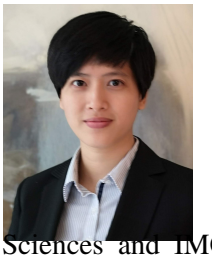

Hongru Chen is an Assistant Professor at Kyushu University, Japan. She received her Bachelor's degree from Northwestern Polytechnical University, China, in 2010, and her Ph.D. from Kyushu University, in 2015, both in aerospace engineering. She did her Ph.D. thesis at ISAS/JAXA, once worked at the Chinese Academy of Sciences and IMCCE/Paris Observatory, and participated in JAXA and CNES planetary projects, such as PROCYON, DESTINY, and MMX. Her research interests include astrodynamics, orbit design, nano-satellite engineering, and atmosphere modeling.

Graphical table of contents

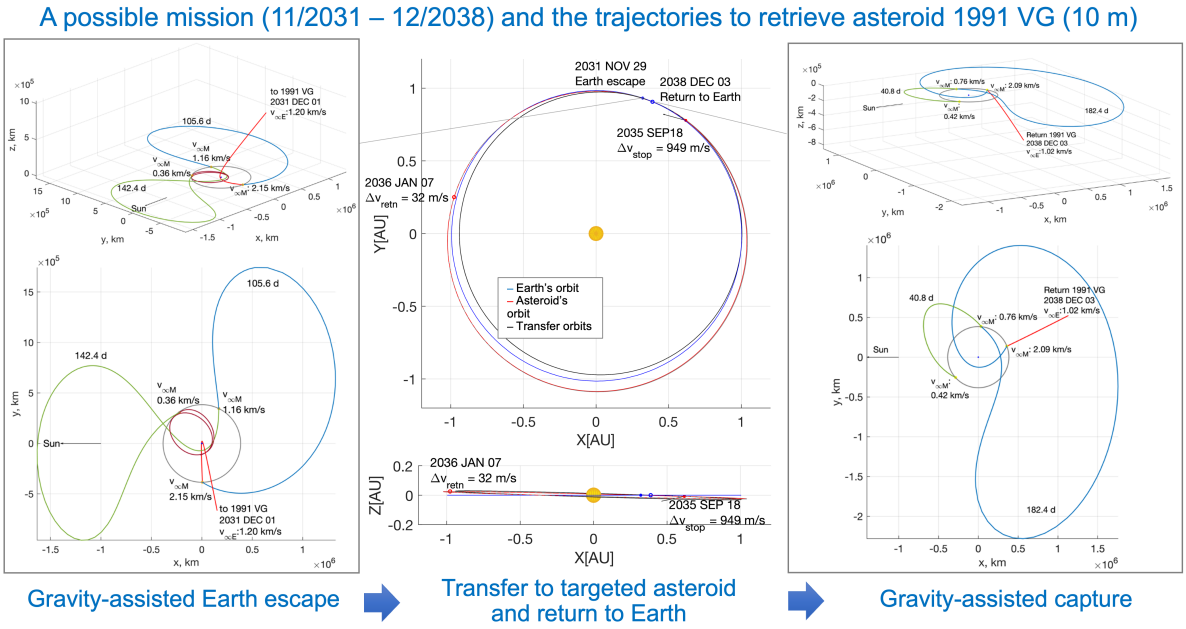

1) Capacity of lunar and solar gravity assists for deep-space mission design is characterized. 2) The trajectory design technique is applied to asteroid flyby, rendezvous, sample return, and retrieval. 3) Various Moon-to-Moon transfer types, namely, the short transfer, Sun-perturbed transfer, multi-revolution transfer, and three-dimensional transfer, are covered.

Fig. 14 Graphical abstract of the paper